PROCEEDINGS OF SCIENCE

Measurement of the primary cosmic-ray proton spectrum between 40 TeV and a few hundred TeV with the Tibet hybrid experiment (Tibet-III + MD)

Y.Katayose[a,*] **on behalf of the Tibet ASγ collaboration**
(a complete list of authors can be found at the end of the proceedings)
[a] *Faculty of Engineering, Yokohama National University, Yokohama 240-8501, Japan*
E-mail: katayose-yusaku-dv@ynu.jp

We have been observing extensive air showers using the Tibet-III air shower array and the underground water-Cherenkov muon detector array (MD) to determine the chemical composition of cosmic rays with energies corresponding to the knee energy region. In previous studies, we developed a method to acquire the proton spectrum in the energy range from 40 to 630 TeV via a hybrid experiment using the Tibet-III and MD and investigated its performance. We conducted Monte Carlo simulations showing that this method can separate protons with a purity of 90% and that the maximum total systematic error of the proton flux depending on interaction models in air-shower development is ±37%. In the present study, analysis results for data acquired over a period of 12 days in 2014 are presented. The abundances of proton-like showers to whole well-reconstructed showers, including model dependence, are 9.1%–14.5% at ∼35 TeV and 1.8%–3.1% at ∼450 TeV.

38th International Cosmic Ray Conference (ICRC2023)
26 July - 3 August, 2023
Nagoya, Japan

ICRC2023
38th International Cosmic Ray Conference
The Astroparticle Physics Conference

*Speaker

PoS(ICRC2023)301

1. Introduction

Cosmic rays (CRs) with energies as high as the petaelectron volt level are generally thought to originate in our galaxy. The acceleration mechanisms, propagation, and source distribution of CRs affect the chemical composition and intensity spectrum of CRs observed on Earth, especially the bent shape of the total particle spectrum at approximately 10^{15} eV (i.e., the "knee region"), which is considered to be due to the acceleration limit of galactic CRs. Therefore, measuring the composition and acquiring the spectra of CRs with energies corresponding to the knee region are critical. Among the spectra, the proton spectrum has been actively investigated in a wide energy range. The proton spectrum in the energy range below 10 TeV has been acquired with high precision mostly through direct observation experiments using balloons and satellites [1–5]. In the energy region below 10 TeV, the spectral shape power is hardened from ∼200 GeV/n [6]. Although several theoretical models have been proposed to explain this phenomenon, such as the influence of a source object near the solar system, its origin has not yet been clarified. For the energy range above 100 TeV, several spectra acquired indirectly, mostly through air-shower observations, have been reported. The Tibet ASγ group have reported that the proton spectrum power index changes over several hundred teraelectron volts [7, 8], indicating a rigidity-dependent acceleration model in which heavier nuclei gradually become dominant with increasing energy. Moreover, the analyses of data from the KASCADE and IceTop experiments have shown that helium becomes dominant [9] and that the proton spectrum power index becomes hard to the petaelectron volt region [10], respectively. At approximately 100 TeV, the measurement is difficult by both direct and indirect methods. The ARGO-YBJ group reported only the proton+helium spectrum in the energy range 3–300 TeV, as acquired with a dense air-shower array [11]. However, the precise proton spectrum has not been reported.

The Tibet ASγ group has been performing a continuous observation to investigate the CR composition around the knee region. The Tibet ASγ detector comprises the surface detector array (Tibet air-shower array; Tibet-III) [12, 13] and the large underground water Cherenkov muon detector array (MD) [14–17]. In the present study, we report preliminary results of the proton spectrum acquired at energies from 40 to 630 TeV using the MD and Tibet-III.

2. Tibet-III and MD

The experimental site of Tibet ASγ is located at Yangbajing Plateau, China (90.522° east, 30.102° north, 4,300 m a.s.l., 606 g/cm^2 atmospheric depth). Its detector comprises the Tibet-III [19], which consists of 597 plastic scintillation detectors, and the MD [14–17]. The Tibet-III covers an area of 65,700 m^2, and detects electromagnetic components, such as electrons and gamma-rays, in air showers; it also measures the particle arrival time and density of shower particles. These data are used to reconstruct the direction of arrival and energy of primary CRs for each event. The MD comprises 64 water Cherenkov-type detectors placed 2.4 m beneath the Tibet-III. Each cell of the MD is a concrete water tank with an area of 7.5 m × 7.5 m and a depth of 1.5 m, with a 20-inch-diameter photomultiplier tube (PMT) mounted downward on the ceiling. The inner surface is coated with white paint so that it acts not only as a waterproof layer but also as a reflector

for Cherenkov photons, which are emitted by air-shower muons and subsequently collected by the PMTs.

3. Data analysis methods and performance evaluation by Monte Carlo simulation

Each surface detector in the Tibet-III measures the number of particles and their arrival times, and the air-shower reconstruction provides the core position, shower arrival direction, and the charged-particle number density (ρ [/m^2]) [19, 28, 29].
To screen well-reconstructed shower events from the entire set of collected data, the following conditions were imposed [18].

1. At least four detectors must be hit within the time width of coincidence of 600 ns.
2. The number of detectors with $\rho \geq 3.5$ must be at least four in the inner detectors of the array.

Here, “inner detectors" refers to the detectors inside the outermost detectors of the AS array.

3. Five or more of the top six detectors with the highest number of detected particles must be contained in the inner detectors.
4. The location of the air-shower core determined by the analysis must be within a 70-m radius from the array center (15,400 m^2).
5. The residual error from the air-shower front, which is defined as a reverse-conic type [8, 30, 31], must be less than 1.0 m.
6. The zenith angle θ must satisfy $\sec\theta < 1.1$.

3.1 Proton separation method and reconstruction of proton spectrum

We have developed a method to acquire proton spectra via a hybrid experiment using the Tibet-III and MD. The details of this method have been reported elsewhere [18]. Here, we briefly summarize the general analysis method.
(1) We divided the reconstructed events into six bins of $\Sigma\rho$ ranging from $10^{2.6}$ to $10^{3.8}$. (2) To separate the proton-like showers, we used the sum of the number of particles measured in each cell of the MD N_μ. We examined the distribution of the number of muons in each $\Sigma\rho$ bin and separated proton-like events with the given purity using a threshold $N_{\mu,\mathrm{cut}}$. (3) To determine the energy of each proton-like event, we used Monte Carlo (MC) data to investigate the relationship between the true energy and $\Sigma\rho$. The peak of the energy distribution was considered the representative energy of the $\Sigma\rho$ bin. The representative energy was determined for each bin and was fitted as a function of $\Sigma\rho$ to obtain a conversion function for energy determination of each shower event. (4) Once the energy of an event identified as proton-like was determined, the flux of the k-th energy bin was given by

$$\frac{dJ}{dE}[/\mathrm{s}/\mathrm{m}^2/\mathrm{sr}/\mathrm{GeV}] = \frac{N_{\mathrm{exp}}^{\text{proton-like}}(k) \times X_{\mathrm{sim}}^{\mathrm{purity}}}{T_{\mathrm{exp}} \times (S\Omega)_{\mathrm{eff}}(k) \times X_{\mathrm{sim}}^{\mathrm{survival}}(k) \times dE(k)} \quad , \tag{1}$$

where T_{exp} denotes the observation time, $X_{\mathrm{sim}}^{\mathrm{survival}}(k)$ denotes the proton survival ratio in the k-th energy bin, and $dE(k)$ denotes the energy bin width. In addition, $N_{\mathrm{exp}}^{\text{proton-like}}(k)$ is the number of events identified as proton-like in the experimental data analysis and $X_{\mathrm{sim}}^{\mathrm{purity}}(= 0.9)$ is the proton purity in the proton-like event. Parameter $(S\Omega)_{\mathrm{eff}}(k)$ is the effective acceptance of the k-th energy bin of the reconstructed proton-induced shower.

3.2 Monte Carlo simulation study of the performance of the proton spectrum measurement

To evaluate the proton survival ratio and the systematic error of proton spectrum measurements with this method, we performed Monte Carlo simulations (MCSs) of air-shower development, assuming multiple combinations of the primary composition model and nuclear cascade model of the air shower. We used the CORSIKA code (version 7.6400) [20] for air-shower generation and the GEANT4.10.02 code to simulate the detector response. In the air-shower simulations, FLUKA [21] was used for low-energy hadronic interactions and three interaction models were compared for the high-energy region. The three models were the SIBYLL 2.3c model [22, 23], the QGSJET-II-04 model [24], and the EPOS Large Hadron Collider (LHC) model [25]. Two models were compared as chemical composition models of primary CRs. First, the "Shibata model" [26], which was obtained by assuming that the CR source has a rigidity-dependent acceleration limit and that the heavier nuclei gradually became dominant from the tens of teraelectron volts region, was used. Second, the "Gaisser-fit model" [27], which was obtained from observation results in which helium was the main component at $\geq$100 TeV, was applied. Thus, we tested a total of six combinations: SIBYLL/FLUKA+Shibata, SIBYLL/FLUKA+Gaisser-fit, QGSJET/FLUKA+Shibata, QGSJET/FLUKA+Gaisser-fit, EPOS_LHC/FLUKA+Shibata, and EPOS_LHC/FLUKA+Gaisser-fit. The MCS showed that the proton spectrum could be measured in the energy range 40–630 TeV if proton-like events with 90% purity were selected. The maximum systematic error included in our analysis due to the interaction model was ±37%. We have summarized the details of the performances elsewhere [18].

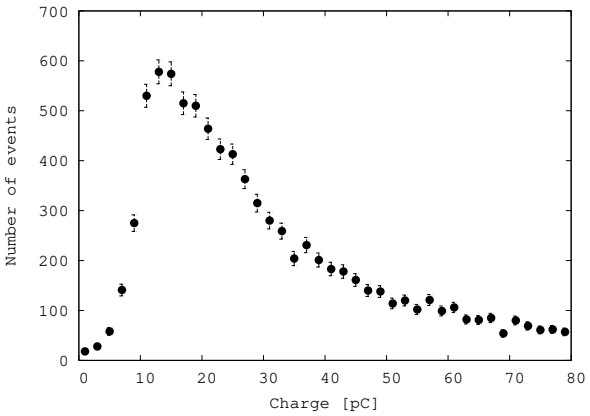

Figure 1: Charge distribution recorded by a PMT in a cell of the MD during a certain 20-minute period. The distribution shows the results of measured muons in air showers that satisfy the conditions described in section 3.

4. Analysis of observation data

Hybrid observations of the Tibet III and MD began in 2014, and observation data have been accumulated continuously. This study analyzed data acquired over a period of 12 days in 2014.
For proton separation using muon numbers, particle-number calibration of the MD is critical. Fig. 1 shows the charge distribution in a PMT in a cell of the MD for reconstructed air-shower events that

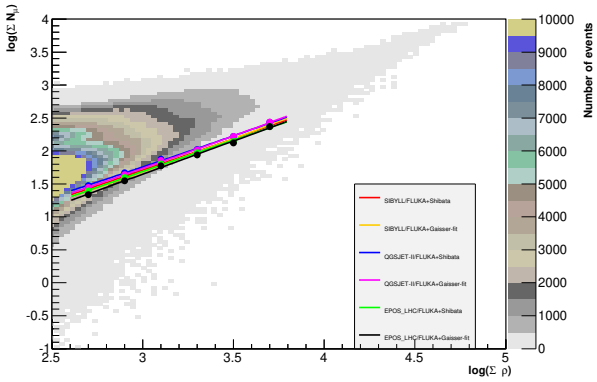

Figure 2: Event intensity map with log $(\sum \rho)$ on the vertical axis and log $(\sum N_\mu)$on the horizontal axis.

satisfy the conditions described in section 3. The muon density is maximal at the AS core and decreases with increasing distance from the shower axis. Thus, the number of muons in many single MD cells is on the order of unity. The peak value of the distribution is used to define a single particle. The experiment calibrates the muon number every 20 min for each MD cell using such a distribution [16].

For proton selection, we used the sum of the number of particles measured in each cell of the MD, N_μ. Fig. 2 is an intensity map of the observed event number over a period of approximately 12 days in 2014. The horizontal axis shows the sum of the charged-particle number density (log $(\sum \rho)$) measured by the Tibet-III, and the vertical axis indicates the number of muons (log $(\sum N_\mu)$) in the shower measured by the MD. To select proton-like events, we divided the data in the figure into six bins of $\Sigma\rho$ ranging from $10^{2.6}$ to $10^{3.8}$ and examined the distribution of muons in each bin. Fig. 3 shows the results for each $\sum \rho$ bin event. The red data points are observed data; the other plots show data obtained from simulations with the SIBYLL/FLUKA+Shiata model. Blue, yellow, and purple data points represent whole events, proton events, and other nuclides, respectively. The solid curves are functions fitted to the MC data [18]. The shoulder peaks in Fig. 3 at N_μ values greater than the peak position are due to the effect of the geometrical configuration of the MD. When the shower core impacts a cell of the MD, more muons are detected than when it does not. The solid lines show each bin's representative cut value $N_{\mu,cut}$ to separate proton-like events with 90% purity. The results show that protons with 90% purity can be selected in all of the $\sum \rho$ regions. The dot in Fig 2 shows the cut values of 90% proton purity in each bin, and the solid lines are the fitted curves [18]. The red dots show cut values determined by simulations using the SIBYLL and FLUKA interaction model and Shibata's composition model. The shape of the N_μ distribution depends on the interaction and composition models; thus, the value of the cut differs for each model. In Fig. 2, the orange, blue, purple, green, and black dots are the results obtained using the SIBYLL/FLUKA+Gaisser-fit model, QGSJET-II/FLUKA+Shiata model, QGSJET-II/FLUKA+Gaisser-fit model, EPOS_LHC/FLUKA+Shibata model, and EPOS_LHC/FLUKA+Gaisser-fit model, respectively. We defined events with $\sum N_\mu$ smaller than this curve as proton-like events. The abundances of proton-like showers to the whole well-reconstructed shower at each $\sum \rho$ is shown in Fig 4. The abundance including model depen-

dence was 9.1–14.5% at $\log(\sum\rho) = 2.7$ and 1.8–3.1% at $\log(\sum\rho) = 3.7$.

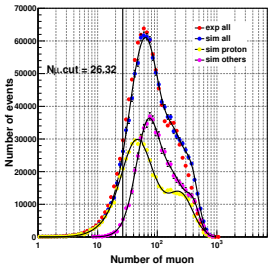

(a) $2.6 \leq \log(\sum\rho) < 2.8$

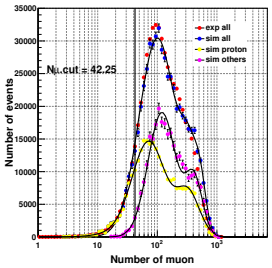

(b) $2.8 \leq \log(\sum\rho) < 3.0$

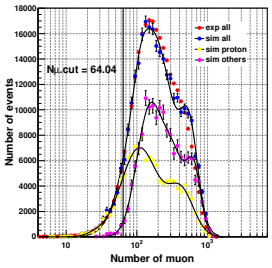

(c) $3.0 \leq \log(\sum\rho) < 3.2$

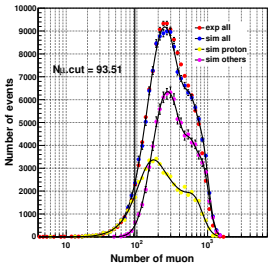

(d) $3.2 \leq \log(\sum\rho) < 3.4$

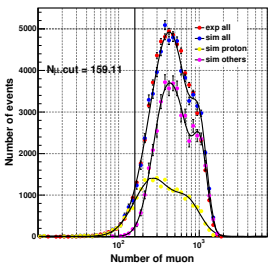

(e) $3.2 \leq \log(\sum\rho) < 3.4$

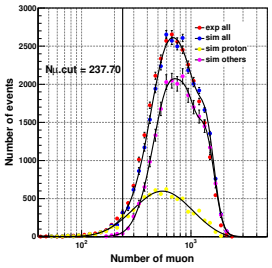

(f) $3.6 \leq \log(\sum\rho) < 3.8$

Figure 3: Muon number distribution for each $\sum\rho$ bin observed for approximately 12 days.

5. Conclusion

The hybrid experiment with the Tibet-III and MD has been accumulating data since 2014 [16]. To measure the proton spectrum in the energy range 40–630 TeV, we analyzed data acquired over a period of 12 days in 2014. The abundances of proton-like showers to whole well-reconstructed

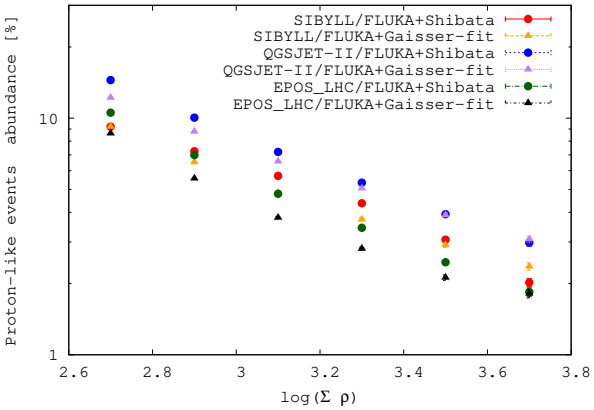

Figure 4: Proton-like shower abundance to whole well-reconstructed showers as a function of log $(\sum \rho)$ for each model when the purity is 90%.

showers, including model dependence, was 9.1–14.5% at ~35 TeV and 1.8–3.1% at ~450 TeV. We expect to use the proposed method to measure the proton spectrum in the 100 TeV region.

Acknowledgements

The collaborative experiment of the Tibet Air Shower Arrays has been conducted under the auspices of the Ministry of Science and Technology of China and the Ministry of Foreign Affairs of Japan. This work was supported in part by a Grant-in-Aid for Scientific Research on Priority Areas from the Ministry of Education, Culture, Sports, Science and Technology, and by Grants-in-Aid for Science Research from the Japan Society for the Promotion of Science in Japan. This work is supported by the National Natural Science Foundation of China under Grants No. 12227804, No. 12275282, No. 12103056 and No. 12073050, and the Key Laboratory of Particle Astrophysics, Institute of High Energy Physics, CAS. This work is also supported by the joint research program of the Institute for Cosmic Ray Research (ICRR), the University of Tokyo.

References

[1] A. D. Panov et al., Bull. Russ. Acad. Sci.: Phys., **71**, 494 (2007).

[2] Y. S. Yoon et al., Astrophys. J., **839**, 5 (2017).

[3] O. Adriani et al., Phys. Rev. Lett., **122**, 181102 (2019).

[4] O. Adriani et al., Phys. Rev. Lett., **129**, 101102 (2019).

[5] Q. An et al., Sci. Adv., **5**, eaax3793 (2019).

[6] N. Tomassetti, ApJ Lett., **752**, L13 (2012).

[7] M. Amenomori et al., Adv. Space Res., **42**, 647 (2008).

[8] M. Amenomori et al., ApJ, **678**, 1165 (2008).

[9] W.D. Apel et al., Astroparticle Phys., **31**, 86 (2009).

[10] K. Rawlins, Phys. At. Nucl., **83**, 280 (2020).

[11] B. Bartoli et al., Phys. Rev. D, **91** 112017 (2015).

[12] M. Amenomori et al., ApJ, **692**, 61 (2009).

[13] M. Amenomori et al., ApJ Lett., **709**, L6 (2010).

[14] T.K. Sako et al., Astroparticle Phys., **32**, 177 (2009).

[15] M. Amenomori et al., ApJ, **813**, 98 (2015).

[16] M. Amenomori et al., Phys. Rev. Lett., **123**, 051101 (2019).

[17] M. Amenomori et al., Phys. Rev. Lett., **126**, 141101 (2021).

[18] D. Kurashige et al., Prog. Theor. Exp. Phys., **2022** , 9, 093F01 (2022)

[19] M. Amenomori et al., ApJ, **598**, 242 (2003).

[20] Heck D. et al., Forschungszentrum Karlsruhe Report FZKA, 6019 (1998).

[21] Battistoni G. et al., Annals of Nuclear Energy, **82**, 10 (2015).

[22] R. Engel et al., EPJ Web of Conferences , **145**, 08001 (2017).

[23] A. Fedynitch et al., Phys. Rev. D, **100**, 103018 (2019).

[24] Ostapchenko S., Nucl. Phys. B (Proc. Suppl.), **151**, 143 (2006).

[25] T. Pierog et al., Phys. Rev. C, **92**, 034906 (2015).

[26] M. Shibata et al., ApJ, **716**, 1076 (2010).

[27] T.K. Gaisser et al., Front. Phys., **8**, 748 (2013).

[28] M. Amenomori et al., Phys. Rev. Lett., **69**, 2468 (1992).

[29] K. Kawata et al., Exp. Astron., **44**, 1 (2017).

[30] S. Kato et al., Exp. Astron., **52**, 85 (2021).

[31] Amenomori, M. et al., Nucl. Instrum. Methods Phys. Res. A, **288**, 619 (1990)

Full Authors List: the Tibet ASγ Collaboration

M. Amenomori[1], Y. W. Bao[2], X. J. Bi[3], D. Chen[4], T. L. Chen[5], W. Y. Chen[3], Xu Chen[4], Y. Chen[2], Cirennima[5], S. W. Cui[6], Danzengluobu[5], L. K. Ding[3], J. H. Fang[3,7], K. Fang[3], C. F. Feng[8], Zhaoyang Feng[3], Z. Y. Feng[9], Qi Gao[5], Q. B. Gou[3], Y. Q. Guo[3], Y. Y. Guo[3], Y. Hayashi[10], H. H. He[3], Z. T. He[6], K. Hibino[11], N. Hotta[12], Haibing Hu[5], H. B. Hu[3], K. Y. Hu[3,7], J. Huang[3], H. Y. Jia[9], L. Jiang[3], P. Jiang[4], H. B. Jin[4], K. Kasahara[13], Y. Katayose[14], C. Kato[10], S. Kato[15], I. Kawahara[14], T. Kawashima[15], K. Kawata[15], M. Kozai[16], Labaciren[5], G. M. Le[17], A. F. Li[3,9,18], H. J. Li[5], W. J. Li[3,10], Y. Li[4], Y. H. Lin[3,7], B. Liu[19], C. Liu[3], J. S. Liu[3], L. Y. Liu[4], M. Y. Liu[5], W. Liu[3], H. Lu[3], T. Makishima[14], Y. Masuda[10], S. Matsuhashi[14], M. Matsumoto[10], X. R. Meng[5], Y. Meng[3,7], A. Mizuno[15], K. Munakata[10], Y. Nakamura[15], H. Nanjo[1], C. C. Ning[5], M. Nishizawa[20], R. Noguchi[14], M. Ohnishi[15], S. Okukawa[14], S. Ozawa[21], X. Qian[4], X. L. Qian[22], X. B. Qu[23], T. Saito[24], M. Sakata[25], T. Sako[15], T. K. Sako[15], T. Sasaki[11], J. Shao[3,9], T. Shibasaki[26], M. Shibata[14], A. Shiomi[26], H. Sugimoto[27], W. Takano[11], M. Takita[15], Y. H. Tan[3], N. Tateyama[11], S. Torii[28], H. Tsuchiya[29], S. Udo[11], R. Usui[14], H. Wang[3], S. F. Wang[5], Y. P. Wang[5], Wangdui[5], H. R. Wu[3], Q. Wu[5], J. L. Xu[4], L. Xue[8], Z. Yang[3], Y. Q. Yao[4], J. Yin[4], Y. Yokoe[15], Y. L. Yu[3,7], A. F. Yuan[5], L. M. Zhai[4], H. M. Zhang[3], J. L. Zhang[3], X. Zhang[2], X. Y. Zhang[8], Y. Zhang[3], Yi Zhang[30], Ying Zhang[3], S. P. Zhao[3], Zhaxisangzhu[5], X. X. Zhou[9] and Y. H. Zou[3,7]

[1]Department of Physics, Hirosaki University, Hirosaki 036-8561, Japan.
[2]School of Astronomy and Space Science, Nanjing University, Nanjing 210093, China.
[3]Key Laboratory of Particle Astrophysics, Institute of High Energy Physics, Chinese Academy of Sciences, Beijing 100049, China.
[4]National Astronomical Observatories, Chinese Academy of Sciences, Beijing 100101, China.
[5]Department of Mathematics and Physics, Tibet University, Lhasa 850000, China.
[6]Department of Physics, Hebei Normal University, Shijiazhuang 050016, China.
[7]University of Chinese Academy of Sciences, Beijing 100049, China.
[8]Institute of Frontier and Interdisciplinary Science and Key Laboratory of Particle Physics and Particle Irradiation (MOE), Shandong University, Qingdao 266237, China.
[9]Institute of Modern Physics, SouthWest Jiaotong University, Chengdu 610031, China.
[10]Department of Physics, Shinshu University, Matsumoto 390-8621, Japan.
[11]Faculty of Engineering, Kanagawa University, Yokohama 221-8686, Japan.
[12]Faculty of Education, Utsunomiya University, Utsunomiya 321-8505, Japan.
[13]Faculty of Systems Engineering, Shibaura Institute of Technology, Omiya 330-8570, Japan.
[14]Faculty of Engineering, Yokohama National University, Yokohama 240-8501, Japan.
[15]Institute for Cosmic Ray Research, University of Tokyo, Kashiwa 277-8582, Japan.
[16]Polar Environment Data Science Center, Joint Support-Center for Data Science Research, Research Organization of Information and Systems, Tachikawa 190-0014, Japan.
[17]National Center for Space Weather, China Meteorological Administration, Beijing 100081, China.
[18]School of Information Science and Engineering, Shandong Agriculture University, Taian 271018, China.
[19]Department of Astronomy, School of Physical Sciences, University of Science and Technology of China, Hefei 230026, China.
[20]National Institute of Informatics, Tokyo 101-8430, Japan.
[21]National Institute of Information and Communications Technology, Tokyo 184-8795, Japan.
[22]Department of Mechanical and Electrical Engineering, Shangdong Management University, Jinan 250357, China.
[23]College of Science, China University of Petroleum, Qingdao 266555, China.
[24]Tokyo Metropolitan College of Industrial Technology, Tokyo 116-8523, Japan.
[25]Department of Physics, Konan University, Kobe 658-8501, Japan.
[26]College of Industrial Technology, Nihon University, Narashino 275-8575, Japan.
[27]Shonan Institute of Technology, Fujisawa 251-8511, Japan.
[28]Research Institute for Science and Engineering, Waseda University, Tokyo 162-0044, Japan.
[29]Japan Atomic Energy Agency, Tokai-mura 319-1195, Japan.
[30]Key Laboratory of Dark Matter and Space Astronomy, Purple Mountain Observatory, Chinese Academy of Sciences, Nanjing 210034, China.

PoS(ICRC2023)301